Ocean Engineering 81 (2014) 1–11

Contents lists available at ScienceDirect

Ocean Engineering

journal homepage: www.elsevier.com/locate/oceaneng

Loading due to interaction of waves with colinear and oblique currents

M. Hasanat Zaman *, Emile Baddour

National Research Council Canada, Arctic Ave., PO Box 12093, St. John's, NL, Canada A1B 3T5

ARTICLE INFO

Article history:
Received 8 April 2013
Accepted 16 February 2014
Available online 5 March 2014

Keywords:
3D wave–current field
Superposition model
Wave–current loading
Moments

ABSTRACT

A study on the loading of an oblique surface wave and a surface current field on a fixed vertical slender cylinder in a 3D flow frame is illustrated in the present paper. The three dimensional expressions describing the characteristics of the combined wave–current field in terms of mass, momentum and energy flux conservation equations are formulated. The parameters before the interaction of the oblique wave-free uniform current and current-free wave are used to formulate the kinematics of the flow field. These expressions are also employed to formulate and calculate the loads imparted by the wave–current combined flow on a bottom mounted slender vertical cylinder. In the present study two different situations are assumed where current is uniform over depth and also acting over a layer of fluid that extends from the free surface to a specified finite depth. In this paper we extend the approach considered in Zaman and Baddour (2004) for the wave–current analysis. Morison et al. (1950) equation is deployed for the load computations in all cases. The above models are utilized to compute the loads and moments on a slender cylinder for a wave with varying range of incidence current field.

1. Introduction

Water motion in the sea is a mixture of wave and current of different forms. The coexistence of waves and currents, their interaction and consequently their loadings on any ocean structures such as gravity-based offshore structure, coastal connecting bridges, coastal recreational establishments and other cylindrical elements of ocean system intersecting the free surface are very important issues for ocean engineers and related scientists to study the stability of the ocean structures. In order to estimate the performance of any ocean structure it is very important for the designer to account for the loading effects resulting from the interaction of a combined wave–current field with any ocean structure.

Longuet-Higgins and Stewart (1960 and 1961), Whitham (1962) derived theoretical expressions for the changes in sea level and other linear and nonlinear characteristics of 2D wave trains by considering momentum flux. Kemp and Simons (1982 and 1983) described the wave–current interactions for following and reverse current. Zaman and Togashi (1996) described their experimental results for interaction of monochromatic wave with favorable and adverse currents over a parabolic bottom structure. Zaman et al. (2008) compared their theoretical and experimental results for interacted wave–current field over a parabolic bottom structure. Zaman et al. (2010) described the interaction of the wave with collinear current. Hedges and Lee (1991) showed that an equivalent uniform current could replace a depth varying current.

In the present model formulation it is assumed that the flow fields are irrotational and inviscid. This allows the estimation of the flow characteristics needed in a Morison et al. (1950) equation context. Velocity potentials are adopted to express the oblique 3D flow fields for: (i) a wave field in the absence of current; (ii) a current field in the absence of wave and (iii) the wave–current combined field after the interaction of both a current-free wave and a wave-free current. These three distinct flow fields are first introduced for collinear flows in Baddour and Song (1990a and 1990b) and extended to 3D in Zaman and Baddour (2003). Zaman and Baddour (2004) showed a comparison of the obtained results due to the present model to those obtained using three other numerical models being used in the offshore industry. These results are shown for a wide range of the normalized current parameters.

For the computation of the parameters of the wave–current field, three-dimensional expressions describing the characteristics of the combined flow in terms of mass, momentum and energy transport conservation equations and the given before-interaction parameters of a wave-free uniform current and current-free wave have been developed. These equations are efficient in describing the combined wave–current field parameters. The relations obtained in satisfying the conservation of mass, momentum, energy flux and a dispersion relation generate a system of nonlinear equations that are solved to evaluate the sought-for wave–current flow parameters, namely, the free surface wave height,

* Corresponding author.
E-mail address: Hasanat.Zaman@nrc-cnrc.gc.ca (M.H. Zaman).

http://dx.doi.org/10.1016/j.oceaneng.2014.02.005
0029-8018

wavelength, current-like term, mean water depth and combined wave–current field direction for a non-collinear case after the interaction. In other words due to the presence of the current the location of the mean water level as well as other parameters of the combined wave–current field will change after the interaction such that to satisfy the conservation equation mentioned above. The concept was generalized for oblique waves in Zaman and Baddour (2002). The obtained model also encompasses the 2D case and is applicable to a current-free or a wave-free flow with appropriate boundary conditions.

In the present computation, we first calculate different parameters of the interacted wave–current field and then use those parameters to calculate the loads imparted by the fluid on a bottom mounted slender vertical cylinder representing a typical element (foundation and substructure of any gravity-based structure (GBS) in the offshore is usually cylindrical) of an offshore structure. For surface currents we also compute moments for current along with loads about the bottom of the cylinder. In this paper the comparisons of computed loads on a slender cylinder by combined wave–current flow field and by superposing wave and current field is shown and discussed. The load computation uses Morison et al. (1950) equation with appropriate drag and mass coefficients given by Iwagaki et al. (1983). See also for example Chakrabarti (1987) and Sarpkaya and Isaacson (1981).

2. Properties of the 3D wave–current field

2.1. Theory

We assume that a current-free monochromatic plane surface wave of wavelength L_o, wave height H_o $(=2a_o)$ and period T propagates over a water body of depth d_o in the direction given by $\vec{N}^w$ and that independently there exists a horizontal uniform wave-free current U_o over the same water depth d_o in the direction $\vec{N}^c$.

When these two plane fields meet, see Fig. 1, a plane of combined wave–current field develops in the direction $\vec{N}$, with a new set of unknown parameters namely, wavelength L, wave height H $(=2a)$, current parameter U and depth d. These unknown parameters together with direction $\vec{N}$ are required to be computed from a system of conservation equations described in the next sections. We first formulate the potential of a wave–current field in a direction $\vec{N}$.

Fig. 1 shows the plan view of the computational domain with O the origin of the 3D inertial frame. The x and y axes subtend the horizontal plane, and z the vertical axis is perpendicular at O to both x and y, and points towards the reader. The unit vectors $\vec{N}^c$, $\vec{N}^w$ and $\vec{N}$ denote the directions of the wave-free current, current-free wave and wave–current plane fields, respectively. The unit vector $\vec{S}$ is normal to $\vec{N}$.

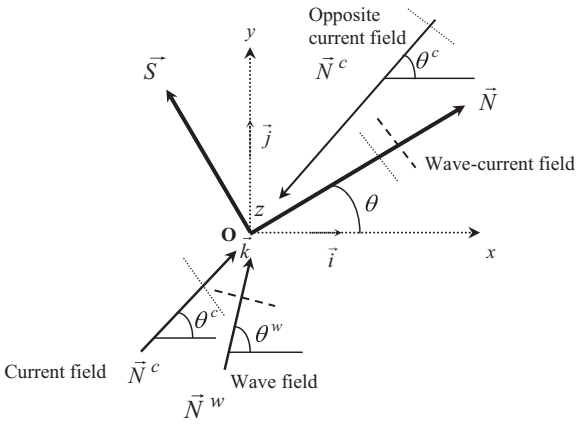

Fig. 1. Wave-free current, current-free wave and wave–current fields relative directions.

Assuming inviscid and incompressible fluid flows we posit that the result of the interaction between a current-free wave with a wave-free current exists and the resulted field is here called a wave–current flow field in the $\vec{N}$ direction. A velocity potential describes this field is given by the following expression to second order in the surface elevation amplitude:

$$\Phi(x,y,z,t)=\vec{U}\times\vec{x}+\frac{a_1}{k\sinh kd}(\sigma-\vec{U}\times\vec{k})\cosh k(d+z)\sin(\vec{k}\times\vec{x}-\sigma t)+\frac{B_H}{k\sinh 2kd}(\sigma-\vec{U}\times\vec{k})\cosh 2k(d+z)\sin 2(\vec{k}\times\vec{x}-\sigma t)+O(k^3a^3) \quad (1)$$

where $B_H=(a_2-(1/2)a_1^2k\coth kd)$ is a parameter related to wave heights, $U=|\vec{U}(U_x,U_y)|$ is the current parameter and $k=|\vec{k}(k_x,k_y)|$ is the wave number whose related vector is normal to the surface elevation front in the wave–current field and lies in the horizontal x–y plane, σ is the angular frequency, a the amplitude of the surface elevation in the wave–current field, d the mean water depth, t the time, $\vec{x}(x,y)$ the horizontal position vector of a point in the field and z is the vertical axis measured vertically upward from the still water level. The first and second order surface elevation amplitudes are given by a_1 and a_2, respectively. Expanding kinematic free surface boundary condition in a Taylor's series about $z=0$ the relationship between a_1 and a_2 can be obtained as:

$$a_2=\pi a_1^2/L(1+(3/2)\sinh^2 kd)\coth kd. \quad (1a)$$

An interested reader can look into, Dean and Dalrymple (1992) for the first order 2D collinear case, and Baddour and Song (1990b) for the second and higher order collinear case.

The relation of the wave number and the angular frequency of the combined wave–current field is given by the following Doppler relation

$$\sigma-\vec{U}\times\vec{k}=\sigma_r \quad (2)$$

where the relative angular frequency in the above equation is described by the following equation:

$$\sigma_r=\sqrt{gk\tanh kd} \quad (3)$$

The dispersion relation for the combined wave–current field is hence

$$(\sigma-\vec{U}\times\vec{k})=\sqrt{gk\tanh kd} \quad (4)$$

The instantaneous free surface elevation η is to first order in amplitude a expressed as:

$$\eta=a\cos(\vec{k}\times\vec{x}-\sigma t)+O(a^2) \quad (5)$$

2.2. Fluid kinematics

The particle velocity components in the x, y and z direction in the combined wave–current field (Eqs. (6)–(8)), current-free wave field (Eqs. (9)–(11)) and wave-free current field (Eqs. (12)–(14)) are obtained as:

$$u_x^{wc}=U_x+\frac{a_1\sigma_r}{\sinh kd}\frac{k_x}{k}\cosh k(d+z)\cos(\vec{k}\times\vec{x}-\sigma t)+\frac{2B_H\sigma_r}{\sinh 2kd}\frac{k_x}{k}\cosh 2k(d+z)\cos 2(\vec{k}\times\vec{x}-\sigma t)+O(k^3a^3) \quad (6)$$

$$u_y^{wc} = U_y + \frac{a_1\sigma_r}{\sinh kd}\frac{k_y}{k}\cosh k(d+z)\cos(\vec{k}\times\vec{x}-\sigma t) + \frac{2B_H\sigma_r}{\sinh 2kd}\frac{k_y}{k}\cosh 2k(d+z)\cos 2(\vec{k}\times\vec{x}-\sigma t)+O(k^3a^3) \quad (7)$$

$$u_z^{wc} = \frac{a_1\sigma_r}{\sinh kd}\sinh k(d+z)\sin(\vec{k}\times\vec{x}-\sigma t) + \frac{2B_H\sigma_r}{\sinh 2kd}\sinh 2k(d+z)\sin 2(\vec{k}\times\vec{x}-\sigma t)+O(k^3a^3) \quad (8)$$

$$u_x^{w} = \frac{a_{o1}\sigma}{\sinh k_od_o}\frac{k_{ox}}{k_o}\cosh k_o(d_o+z)\cos(\vec{k}_o\times\vec{x}-\sigma t) + \frac{2B_{oH}\sigma}{\sinh 2k_od_o}\frac{k_{ox}}{k_o}\cosh 2k_o(d_o+z)\cos 2(\vec{k}_o\times\vec{x}-\sigma t)+O(k_o{}^3a_o{}^3) \quad (9)$$

$$u_y^{w} = \frac{a_{o1}\sigma}{\sinh k_od_o}\frac{k_{oy}}{k_o}\cosh k_o(d_o+z)\cos(\vec{k}_o\times\vec{x}-\sigma t) + \frac{2B_{oH}\sigma}{\sinh 2k_od_o}\frac{k_{oy}}{k_o}\cosh 2k_o(d_o+z)\cos 2(\vec{k}_o\times\vec{x}-\sigma t)+O(k_o{}^3a_o{}^3) \quad (10)$$

$$u_z^{w} = \frac{a_{o1}\sigma}{\sinh k_od_o}\sinh k_o(d_o+z)\sin(\vec{k}_o\times\vec{x}-\sigma t) + \frac{2B_{oH}\sigma}{\sinh 2k_od_o}\sinh 2k_o(d_o+z)\sin 2(\vec{k}_o\times\vec{x}-\sigma t)+O(k_o{}^3a_o{}^3) \quad (11)$$

$$u_x^{c} = U_x \quad (12)$$

$$u_y^{c} = U_y \quad (13)$$

$$u_z^{c} = 0 \quad (14)$$

where $B_{oH} = (a_{o2} - (1/2)a_{o1}^2k_o\coth k_od_o)$, superscripts w, c and wc in the above equations, stand for the quantities in the pre-interaction current-free wave field, wave-free current field and in the post-interaction wave–current field, respectively.

The corresponding acceleration components in the x, y and z directions in the combined wave–current field (Eqs. (15)–(17)), current-free wave field (Eqs. (18)–(20)) and wave-free current field (Eqs. (21)–(23)) are evaluated as:

$$a_x^{wc} = \frac{a_1\sigma_r\sigma}{\sinh kd}\frac{k_x}{k}\cosh k(d+z)\sin(\vec{k}\times\vec{x}-\sigma t) + \frac{4B_H\sigma_r\sigma}{\sinh 2kd}\frac{k_x}{k}\cosh 2k(d+z)\sin 2(\vec{k}\times\vec{x}-\sigma t)+O(k^3a^3) \quad (15)$$

$$a_y^{wc} = \frac{a_1\sigma_r\sigma}{\sinh kd}\frac{k_y}{k}\cosh k(d+z)\sin(\vec{k}\times\vec{x}-\sigma t) + \frac{4B_H\sigma_r\sigma}{\sinh 2kd}\frac{k_y}{k}\cosh 2k(d+z)\sin 2(\vec{k}\times\vec{x}-\sigma t)+O(k^3a^3) \quad (16)$$

$$a_z^{wc} = -\frac{a_1\sigma_r\sigma}{\sinh kd}\sinh k(d+z)\cos(\vec{k}\times\vec{x}-\sigma t) - \frac{4B_H\sigma_r\sigma}{\sinh 2kd}\sinh 2k(d+z)\cos 2(\vec{k}\times\vec{x}-\sigma t)+O(k^3a^3) \quad (17)$$

$$a_x^{w} = \frac{a_1\sigma_r\sigma_r}{\sinh kd}\frac{k_x}{k}\cosh k(d+z)\sin(\vec{k}\times\vec{x}-\sigma t) + \frac{4B_H\sigma_r\sigma_r}{\sinh 2kd}\frac{k_x}{k}\cosh 2k(d+z)\sin 2(\vec{k}\times\vec{x}-\sigma t)+O(k^3a^3) \quad (18)$$

$$a_y^{w} = \frac{a_1\sigma_r\sigma_r}{\sinh kd}\frac{k_y}{k}\cosh k(d+z)\sin(\vec{k}\times\vec{x}-\sigma t) + \frac{4B_H\sigma_r\sigma_r}{\sinh 2kd}\frac{k_y}{k}\cosh 2k(d+z)\sin 2(\vec{k}\times\vec{x}-\sigma t)+O(k^3a^3) \quad (19)$$

$$a_z^{w} = -\frac{a_1\sigma_r\sigma_r}{\sinh kd}\sinh k(d+z)\cos(\vec{k}\times\vec{x}-\sigma t) - \frac{4B_H\sigma_r\sigma_r}{\sinh 2kd}\sinh 2k(d+z)\cos 2(\vec{k}\times\vec{x}-\sigma t)+O(k^3a^3) \quad (20)$$

$$a_x^{c} = 0 \quad (21)$$

$$a_y^{c} = 0 \quad (22)$$

$$a_z^{c} = 0 \quad (23)$$

The pressure distribution in the wave–current field to second order is obtained from the dynamic free surface boundary condition as:

$$P = -\rho gz - \frac{\rho ga^2k}{2\sinh 2kd}[\cosh 2k(d+z)-1] + \rho ga\frac{\cosh k(d+z)}{\cosh kd}\cos(\vec{k}\times\vec{x}-\sigma t) + \frac{3\rho ga^2k}{2\sinh 2kd}\left[\frac{\cosh 2k(d+z)}{\sinh^2 kd}\right] - \frac{\rho ga^2k}{2\sinh 2kd} \quad (24)$$

2.3. Derivation of mass, momentum and energy flux equation

We can obtain the mass flux of the combined wave–current field along the $z-\vec{N}$ vertical plane through the following relation up to the second order in amplitude a (for details see Zaman et al. (2010))

$$Q^{wc} = \frac{1}{2\pi}\int_0^{2\pi}\int_{-d}^{\eta}[\Phi_x+\Phi_y]\,dz\,d\theta \quad (25)$$

$$\vec{Q}^{wc} = \rho d\vec{U} + \frac{\rho a^2}{2}\vec{k}\left(C - \frac{\vec{U}\times\vec{k}}{k}\right)\coth kd + O(k^3a^3) \quad (26)$$

The corresponding momentum flux of the combined wave–current field along the same $z-\vec{N}$ plane is given as follows:

$$M^{wc} = \frac{1}{2\pi}\int_0^{2\pi}\int_{-d}^{\eta}\left[P(x,y,z,t)+\rho\Phi_x^2(x,y,z,t)+\rho\Phi_y^2(x,y,z,t)\right]dz\,d\theta \quad (27)$$

$$\vec{M}^{wc} = \frac{1}{2}\rho ga^2\left(\frac{1}{2}+\frac{2kd}{\sinh 2kd}+\frac{2\vec{U}\times\vec{k}}{\sigma_r}\right) + \frac{1}{2}\rho gd^2\left(1+\frac{2|\vec{U}|^2}{gd}\right)+O(k^3a^3) \quad (28)$$

In a similar fashion the net energy flux of the combined wave–current field in the direction of flow in the $z-\vec{N}$ plane is expressed as:

$$E_j^{wc} = \frac{1}{2\pi}\int_0^{2\pi}\int_{-d}^{\eta}\left[\left\{P+\frac{\rho}{2}(\Phi_x^2+\Phi_y^2+\Phi_z^2)\right\}+\rho gz\right]\Phi_j\,dz\,d\theta \quad : \quad j=x,\ y \quad (29)$$

$$\vec{E}^{wc} = \frac{\rho g\vec{U}}{2}a^2 + \frac{\rho\vec{U}d}{2}\left[|\vec{U}|^2+\frac{gk}{\sinh 2kd}a^2\right] + \frac{\rho ga^2}{4}\left[1+\frac{2kd}{\sinh 2kd}\right]\left[C_r+\frac{\vec{U}\times\vec{k}}{k}\right]\frac{\vec{k}}{k} + \frac{\rho ga^2}{4\sigma_r}\left[2\vec{U}(\vec{U}\times\vec{k})+\vec{k}|\vec{U}|^2\right]+O(k^3a^3) \quad (30)$$

where $\vec{k}/k = \vec{N}$ and $\vec{U}/U = \vec{N}$.

2.4. Conservation equation and numerical method

The following two sets of conservation equations for mass, momentum and energy flux in the $\vec{N}$ and $\vec{S}$ directions, respectively are obtained when the time averages of the above flux of the

current-free wave field, wave-free current field and wave–current field are considered

$$Q^w\vec{N}^w \times \vec{N} + Q^c\vec{N}^c \times \vec{N} = Q^{wc}\vec{N} \times \vec{N} \tag{31}$$

$$M^w\vec{N}^w \times \vec{N} + M^c\vec{N}^c \times \vec{N} = M^{wc}\vec{N} \times \vec{N} \tag{32}$$

$$E^w\vec{N}^w \times \vec{N} + E^c\vec{N}^c \times \vec{N} = E^{wc}\vec{N} \times \vec{N} \tag{33}$$

$$Q^w\vec{N}^w \times \vec{S} + Q^c\vec{N}^c \times \vec{S} = 0 \tag{34}$$

$$M^w\vec{N}^w \times \vec{S} + M^c\vec{N}^c \times \vec{S} = 0 \tag{35}$$

$$E^w\vec{N}^w \times \vec{S} + E^c\vec{N}^c \times \vec{S} = 0 \tag{36}$$

The directional vectors are denoted by the following expression:

$$\vec{N}^w = \cos\theta^w\ \vec{i} + \sin\theta^w\ \vec{j} \tag{37}$$

$$\vec{N}^c = \cos\theta^c\ \vec{i} + \sin\theta^c\ \vec{j} \tag{38}$$

$$\vec{N} = \cos\theta\ \vec{i} + \sin\theta\ \vec{j} \tag{39}$$

$$\vec{S} = -\sin\theta\ \vec{i} + \cos\theta\ \vec{j} \tag{40}$$

and $\vec{N}^w$ and $\vec{N}^c$ are the given wave and current directions; $\vec{N}$ is the final direction of the combined wave–current field and $\vec{S}$ is the direction normal to $\vec{N}$. θ^w and θ^c are the given current-free wave direction and wave-free current direction prior to interaction and θ is the final direction of the combined wave–current field after interaction with the x-horizontal axis.

The vector relationships mentioned in Eqs. (37)–(40) are utilized in the derivation of the conservation of mass, momentum and energy equations in the respective sections.

2.5. Variables declaration

The known and unknown parameters used in this formulation are normalized and defined in the following way:

Normalized known parameters

$$A = \frac{a_o^2}{d_o^2};\quad B = \frac{U_o}{C_o};\quad D = \frac{L_o}{d_o};\quad \theta(\text{not normalized}) \tag{41}$$

Normalized unknown parameters

$$W = \frac{d}{d_o};\quad X = \frac{U}{C_o};\quad Y^2 = \frac{L}{L_o};\quad Z = \frac{a^2}{d_o^2};\quad \tan\theta \tag{42}$$

2.6. Dispersion relation

The normalized dispersion relation (Eq. (4)) for the combined wave–current field can be rewritten in the following form

$$Y^2 - X - Y\left[\tanh(2\pi W/DY^2)\coth(2\pi/D)\right]^{1/2} = 0 \tag{43}$$

2.7. Conservation of mass

The mean rate of transfer of mass across a vertical plane due to the current-free wave field, wave-free current field and combined wave–current field can be written from Eq. (26) in the following forms

$$\vec{Q}^w = Q^w\vec{N}^w = \frac{\rho g a_o^2}{2} C_o \coth(k_o d_o)\, k_o \vec{N}^w \tag{44}$$

$$\vec{Q}^c = Q^c\vec{N}^c = \rho d_o U_o \vec{N}^c \tag{45}$$

$$\vec{Q}^{wc} = Q^{wc}\vec{N} = \rho d U\vec{N} + \frac{\rho a^2}{2}\coth(kd)\left(C - \frac{\vec{U}\times\vec{k}}{k}\right)k\vec{N} \tag{46}$$

Inserting Eqs. (44)–(46) into Eq. (31) and after normalization the following equation would be obtained to express the conservation of mass in the $\vec{N}$ direction

$$\pi A\coth(2\pi/D)\cos(\theta^w-\theta) + DB\cos(\theta^c-\theta) - DWX - \pi\frac{Z}{Y}\left[\coth(2\pi W/DY^2)\coth(2\pi/D)\right]^{\frac{1}{2}} = 0 \tag{47}$$

From Eq. (34) the conservation of mass equation in the $\vec{S}$ direction could be obtained in the following way

$$\pi A\coth(2\pi/D)\sin(\theta^w-\theta) + DB\sin(\theta^c-\theta) = 0 \tag{48}$$

2.8. Conservation of momentum

The mean rate of transfer of momentum due to the current-free wave field, wave-free current field and combined wave–current field can be written using Eq. (28) in the following way

$$M^w\vec{N}^w = \left[\frac{1}{2}\rho g a_o^2\left(\frac{1}{2} + \frac{2k_o d_o}{\sinh(2k_o d_o)}\right) + \frac{1}{2}\rho g d_o^2\right]\vec{N}^w \tag{49}$$

$$M^c\vec{N}^c = \rho d_o\left|\vec{U}_o\right|^2\vec{N}^c \tag{50}$$

$$M^{wc}\vec{N} = \left[\frac{1}{2}\rho g a^2\left(\frac{1}{2} + \frac{2kd}{\sinh(2kd)} + \frac{2\vec{U}\times\vec{k}}{\sigma_r}\right) + \frac{1}{2}\rho g d^2\left(1 + \frac{2\left|\vec{U}\right|^2}{gd}\right)\right]\vec{N} \tag{51}$$

Substituting Eqs. (49)–(51) into Eq. (32) and after normalization the conservation of the momentum equation in the $\vec{N}$ direction would be obtained as follows:

$$\left[1 + A\left(\frac{1}{2} + \frac{2\pi/D}{\sinh(2\pi/D)\cosh(2\pi/D)}\right)\right]\cos(\theta^w-\theta) + \frac{D}{\pi}B^2\tanh(2\pi/D)\cos(\theta^c-\theta) - W^2 - Z\left(\frac{1}{2} + \frac{2\pi W/DY^2}{\sinh(2\pi W/DY^2)\cosh(2\pi W/DY^2)}\right) - 2\frac{XZ}{Y}\sqrt{\tanh(2\pi/D)\coth(2\pi W/DY^2)} - \frac{DW}{\pi}X^2\tanh(2\pi/D) = 0 \tag{52}$$

From Eq. (35), the normalized conservation of momentum equation in the $\vec{S}$ direction could be obtained in the following form

$$\left[1 + A\left(\frac{1}{2} + \frac{2\pi/D}{\sinh(2\pi/D)\cosh(2\pi/D)}\right)\right]\sin(\theta^w-\theta) + \frac{D}{\pi}B^2\tanh(2\pi/D)\sin(\theta^c-\theta) = 0 \tag{53}$$

2.9. Conservation of energy

The mean rate of transfer of energy due to the current-free wave field, wave-free current field and combined wave–current field can be written using Eq. (30)

$$E^w\vec{N}^w=\frac{\rho g a_o^2}{4}C_o\left[1+\frac{2k_od_o}{\sinh(2k_od_o)}\right]\frac{\vec{k}_o}{k_o}\vec{N}^w \tag{54}$$

$$E^c\vec{N}^c=\frac{\rho d_o\left|\vec{U}\right|^2}{2}\vec{U}\vec{N}^c \tag{55}$$

$$\begin{aligned}E^{wc}\vec{N}=&\frac{\rho g\vec{U}}{2}a^2\vec{N}+\frac{\rho\vec{U}d}{2}\left[\left|\vec{U}\right|^2+\frac{gk}{\sinh(2kd)}a^2\right]\vec{N}\\&+\frac{\rho g a^2}{4}\left[1+\frac{2kd}{\sinh(2kd)}\right]\left[\left(C_r+\frac{\vec{U}\times\vec{k}}{k}\right)\right]\frac{\vec{k}}{k}\vec{N}\\&+\frac{\rho g a^2}{4\sigma_r}\left[2\vec{U}(\vec{U}\times\vec{k})+\vec{k}\left|\vec{U}\right|^2\right]\vec{N}\end{aligned} \tag{56}$$

Introducing Eqs. (54)–(56) into Eq. (33) and after normalization the conservation of the energy equation in the $\vec{N}$ direction would be obtained as:

$$\begin{aligned}&A\left[1+\frac{2\pi/D}{\sinh(2\pi/D)\cos(2\pi/D)}\right]\cos(\theta^w-\theta)\\&+\frac{D}{\pi}\tanh(2\pi/D)B^3\cos(\theta^c-\theta)-2ZX\\&-\frac{DW}{\pi}\tanh(2\pi/D)\\&\left[X^2+2\pi^2\frac{Z}{D^2Y^2}\frac{1}{\tanh(2\pi/D)\sinh(2\pi W/DY^2)\cosh(2\pi W/DY^2)}\right]X\\&-Z\left[1+\frac{2\pi W/DY^2}{\sinh(2\pi W/DY^2)\cosh(2\pi W/DY^2)}\right]\\&\left[Y\left\{\tanh(2\pi W/DY^2)\coth(2\pi/D)\right\}^{1/2}+X\right]\\&-3\frac{X^2Z}{Y}\left[\tanh(2\pi/D)\coth(2\pi W/DY^2)\right]^{1/2}=0\end{aligned} \tag{57}$$

Finally, from Eq. (36) the normalized conservation of energy equation in the $\vec{S}$ direction could be obtained in the following form

$$\begin{aligned}&A\left[1+\frac{2\pi/D}{\sinh(2\pi/D)\cos(2\pi/D)}\right]\sin(\theta^w-\theta)\\&+\frac{DB^3}{\pi}\tanh(2\pi/D)\sin(\theta^c-\theta)=0\end{aligned} \tag{58}$$

2.10. Forms of Morison's equations

The forms of Morison's equations (Morison et al., 1950) used in the load computations are given by the following expressions (Chakrabarti, 2005)

$$\vec{F}_I=C_MA_m\frac{D\vec{u}}{Dt} \tag{59}$$

$$\vec{F}_D=C_DA_d\,\vec{u}\left|\vec{u}\right| \tag{60}$$

where $A_m=(\rho\pi/4)d^2$, $A_d=(\rho/2)d$; C_M and C_D are inertia and drag coefficients, ρ the fluid density and d is the diameter of the cylinder. $D/Dt=\partial/\partial t+u\partial/\partial x+v\partial/\partial y+w\partial/\partial z$ is the time derivative, where u_x, u_y and u_z are the particle velocity components of $\vec{u}$ in the x, y and z directions, respectively.

The coefficients C_M and C_D are obtained for a specific Keulegan–Carpenter (KC) number from the curve proposed by Iwagaki et al. (1983). The total load $\vec{F}_t$ is then obtained from the summation of the inertia and the drag loads as:

$$\vec{F}_t=\vec{F}_I+\vec{F}_D \tag{61}$$

where $\vec{F}_I$ is the load due to inertia and $\vec{F}_D$ is the load due to drag.

The KC number is a measure of the importance of drag load effect is defined by the following equations:

$$KC=\vec{u}_{\max}T/d \tag{62}$$

where T is the wave period and $\vec{u}_{\max}$ is the maximum particle velocity in the x, y and z directions, respectively.

3. Numerical simulation

3.1. Computational procedure

Eqs. (43), (47), (52), (57), (48), (53) and (58) are the required two sets of equations for the evaluations of the properties of the combined wave–current field that results when a current-free wave and a wave-free current interact in a 3D flow field.

At the beginning of the computation the knowledge of the direction of the combined wave–current field is necessary. An iterative solution of any one of the three Eqs. (48), (53) or (58) will give the direction of the combined wave–current field after the interaction. Once the direction of the combined flow is estimated then the system of the nonlinear Eqs. (43), (47), (52) and (57) can be solved iteratively for the required variables W, X, Y and Z. When the variables are known then the computations of the unknown combined wave–current field parameters, a, k, d and U are carried out.

A Newton iterative method has been utilized in this study. For a given wave with parameters a_o, k_o, d_o and current velocity U_o, the computation of the parameters a, k, d and U of the combined wave–current field are carried out from the above equations with a suitable initial guess of the unknowns necessary for iteration to start. If it is assumed that $\theta^w=\theta^c=\theta=0$ then the above 3D numerical model becomes a 2D wave–current model discussed in Zaman and Baddour (2006) and Zaman et al. (2008).

3.2. Computational environment

Maple-12 (2008) release is used for the numerical simulations in this work. Maple is a symbolic programming language using Windows environment. It is used for implementing Newton's algorithm for the numerical solution of the conservation equations together with the dispersion relation. Maple's basic system, or kernel, is sufficiently compact and efficient to be practical for use in a shared environment or on a personal computer. One of the advantages of Maple is that the user can see an equation in its expanded mathematical format on the monitor while it is taking part in the computations.

4. Implementation of 2D and 3D models for uniform current extended from free surface to bottom

Two different numerical models have been used in this study where 2D and 3D models are our proposed model and, S2D and S3D are superposition models. In 2D and 3D models, the total load is calculated from the kinematics of the combined wave–current field. In this case Eqs. (6)–(8), (15)–(17), (43), (47), (52) and (57) will predict the wave–current parameters and Eq. (61) would

Table 1
Description of computational methods.

Models	Kinematics	Load computed
2D model *3D model*	For combined wave and current field	For combined wave and current field
S2D model *S3D model*	For current-free wave field For wave-free current field	For current-free wave field + For wave-free current field

Table 2
Computational parameters.

Parameters	2D model	3D model
U_o/C_o *(Maximum opposing)*	−0.20	−0.20
U_o/C_o *(Maximum following)*	0.572	1.359
H_o/L_o	0.01	0.01
d_o/L_o	2.0	2.0
Wave incident direction	0°	10°
Current incident direction	0°	15°

produce the total load exerted on the cylinder by the combined wave–current field.

S2D and S3D are superposition models where the individual components of the loads on the cylinder, due to a current-free wave and a wave-free current, are separately evaluated and a summation of both loads is then made. Eqs. (9)–(11), (18)–(20), (43), (47), (52) and (57) would be used to compute the kinematics of the current-free wave field and then Eq. (61) is deployed for the computation of the load exerted by the current-free wave. Again when the kinematics of the current field are known from Eqs. (12)–(14), (21)–(23), (43), (47), (52) and (57) then Eq. (61) will give the load due to the wave-free current field. An appropriate summation is then made to obtain the total load. A description of the computational methods is shown in Table 1.

4.1. Case study: Comparisons of loads by 2D and 3D models with corresponding S2D and S3D models

As an example, the established models have been applied for the computation of loads for a collinear or 2D case and for an oblique or 3D case. For both examples, it is assumed that a monochromatic current-free surface wave interacts with a normalized wave-free uniform current U_o/C_o varying over the range of an opposite current to a range of following currents. The wave and current parameters used in this study are shown in Table 2. Subscript 0 denotes a value of a parameter before interaction. The diameter of the cylinder is 35 cm in all computations.

In this comparison Table 2 is used for the computational parameters. In the table H_o and L_o are the current-free wave height and wavelength, respectively.

4.1.1. Load computation by the 2D and S2D models

Figs. 2 and 3 show simple comparison of the wave heights and wavelengths, respectively obtained by the 2D model, experiments by Zaman and Togashi (1996) and experiments by Thomas (1981). However, in Fig. 3 the experimental data of wavelengths by Zaman and Togashi is not available. In this case the predicted and observed wave height H is normalized by the current-free wave height, H_o and the predicted and observed wavelength L is normalized by the current-free wavelength L_o. A good match of the model results with experiments is observed.

Descriptions of maximum and minimum loads obtained by the above two models for 2D collinear, non-oblique case are given in Figs. 4 and 5, respectively. In the 2D case we have found that the

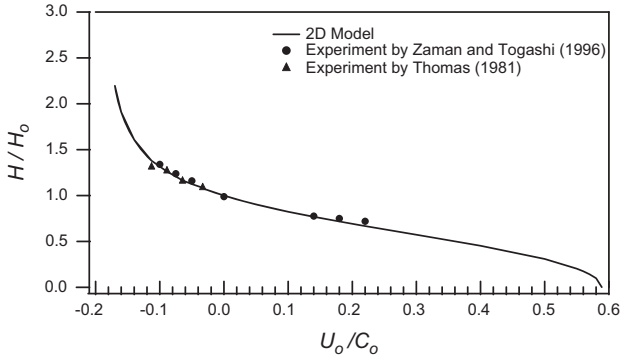

Fig. 2. Comparison of the wave heights obtained from the 2D numerical model with experiments.

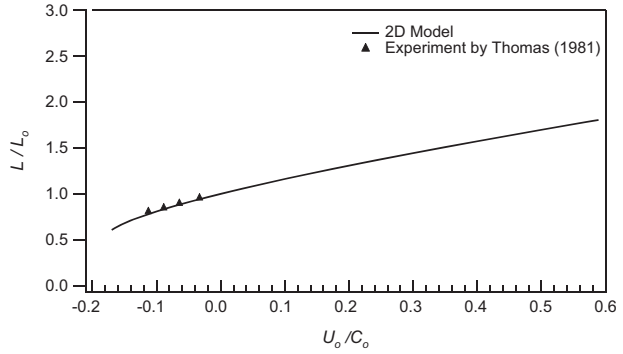

Fig. 3. Comparison of the wavelengths obtained from the 2D numerical model with experiments.

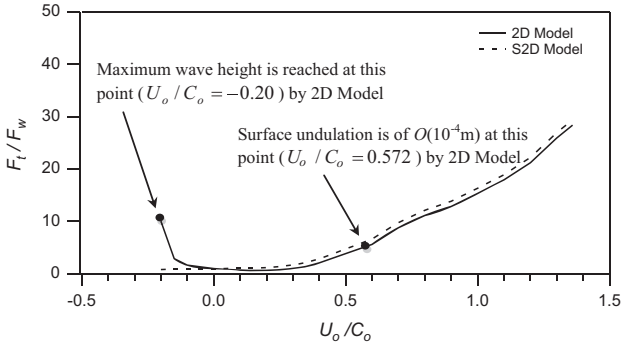

Fig. 4. Normalized maximum exerted loads computed by 2D Model and S2D Model.

monochromatic wave height is of $O(10^{-4}\,\mathrm{m})$ in 2D model when normalized current parameter reaches the value $U_o/C_o = 0.572$ for the case of a wave with a following current. For the case when wave and current are in the opposite direction the maximum wave height is reached at $U_o/C_o = -0.20$. Maximum wave height is reached due to wave blocking. At this point wave steepness

exceeds the allowable breaking value (~0.14) and the numerical model is stopped.

These limits are shown in Figs. 4 and 5 by a black-circle. The analyses and comparisons of loads for 2D non-oblique case are made at these two points, that is, when $U_o/C_o=0.572$ and $U_o/C_o=-0.20$. In the figures and tables F_t stands for the total load due to combined wave–current field or due to wave-free current field and F_w describes the load due to current-free wave field. In Figs. 4 and 5, it may be observed that when waves and currents are in the same direction, that is, U_o/C_o is positive, then for the given, before interaction wave and current conditions, the maximum load obtained at $U_o/C_o=0.572$ by the S2D model is 17.79% larger than that obtained by 2D model. In all cases, Eq. (63) is used to compare the loads obtained by the combined wave–current model (2D or 3D) to the loads that obtained by the relevant superposition wave and current model (S2D or S3D) in %.

$$\% = \frac{R_c - R_s}{R_s} \times 100 \tag{63}$$

where R_c is the load obtained by the combined wave–current model and R_s is the relevant load obtained by the superposition wave and current model.

Again for the minimum load shown in Fig. 5, S2D model yields 17.82% smaller load than 2D model. The above results are summarized in Table 3. A plus sign or a minus sign in the bracket after the percentage value means whether the respective model returns a greater or a smaller load when compare to 2D model.

On the other hand when wave and current are in opposite directions the maximum load obtained at $U_o/C_o=-0.20$ by S2D model is 91.91% smaller than the load obtained by 2D model. Again for the minimum load, S2D model yields 88.55% smaller load than 2D model. Table 4 captures the above findings.

The possibility of such behavior is that in S2D model, the wave heights and the wavelengths are not affected by the interaction since wave and current kinematics are computed separately using before interaction parameters. That is no action of wave on current and vice versa is accounted for. On the other hand, in 2D model, the kinematics is computed from the combined wave–current field where the interaction of wave and current is taken into account. This produces a significant change in wave heights and wavelengths. It is evident that a following current reduces the wave heights and increases the wavelengths. A substantial increase in wave heights and decrease in wavelengths are observed in the waveform for the case of an opposite current. So for the case of a wave interacting with a reverse current, the increase in the wave heights is considered to be responsible for the rapid increase of the loads in a combined wave–current field.

It is important to mention here that when wave and current are in the same direction the wave height reduces with current and disappears when the current is strong enough to eliminate the wave amplitude from the combined wave–current field. In the absence of waves the model is still capable to compute the loading imparted by the wave-free current field. The continuation of the solid line (for 2D model) in the figures after the black-circle, describes the loading due to wave-free current field in this case.

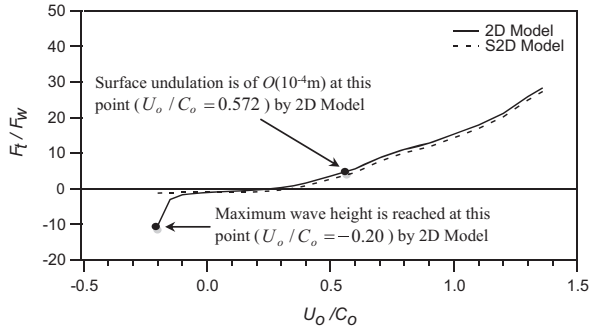

Fig. 5. Normalized minimum exerted loads computed by 2D Model and S2D Model.

Table 3
Loads for 2D case: wave with following current.

	U_o/C_o	F_t/F_w [a]	%
2D model	0.572	5.614	
S2D model	0.572	6.613	17.79 (+)
	U_o/C_o	F_t/F_w [b]	%
2D model	0.572	5.614	
S2D model	0.572	4.613	17.82 (−)

[a] Normalized maximum load.
[b] Normalized minimum load.

Table 4
Loads for 2D case: wave with opposing current.

	U_o/C_o	F_t/F_w [a]	%
2D model	−0.20	10.029	
S2D model	−0.20	0.811	91.91 (−)
	U_o/C_o	F_t/F_w [b]	%
2D model	−0.20	−10.389	
S2D model	−0.20	−1.188	88.55 (−)

[a] Normalized maximum load.
[b] Normalized minimum load.

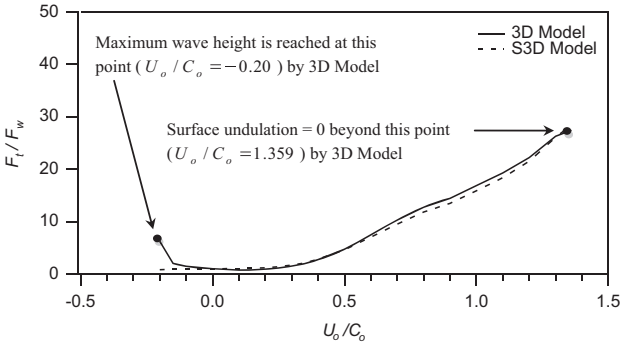

Fig. 6. Normalized maximum exerted loads computed by 3D Model and S3D Model.

4.1.2. Load computation by the 3D and S3D models

For the oblique interaction cases the above mentioned wave and current conditions are used (as shown in Table 2) and in addition, it is assumed that the wave enters the computational domain at an oblique angle of 10°, while the current is at an angle of 15° with the positive direction of the *x*-axis.

Figs. 6 and 7 demonstrate the comparison between the maximum and minimum loads obtained by the above two models in the oblique 3D field. In the 3D oblique case, the analyses and comparisons of loads are also made at two points, at $U_o/C_o=1.359$ when surface elevation is of $O(10^{-4}\,\mathrm{m})$ for a wave with a following current and at $U_o/C_o=-0.20$ when the wave is in opposite direction of the current. In Figs. 6 and 7, it may be perceived that when waves and currents are in the same direction, that is, U_o/C_o is positive, then for the given wave and current parameters the maximum load obtained at $U_o/C_o=1.359$ by S3D model is 0.70% smaller than that obtained by 3D model. Again for minimum load,

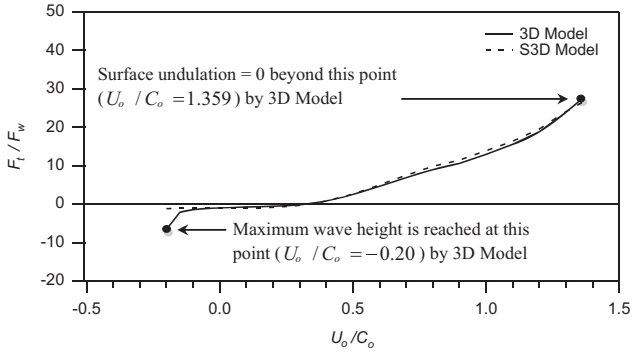

Fig. 7. Normalized minimum exerted loads computed by 3D Model and S3D Model.

Table 5
Loads for 3D case: wave with following current.

	U_o/C_o	F_t/F_w[a]	%
3D model	1.359	26.280	
S3D model	1.359	26.085	0.700 (−)
	U_o/C_o	F_t/F_w[b]	%
3D model	1.359	23.856	
S3D model	1.359	24.085	0.960 (+)

[a] Normalized maximum load.
[b] Normalized minimum load.

S3D model yields 0.96% larger load than 3D model. Table 5 summarizes the above results.

On the other hand, when wave and current are in opposite directions the maximum load obtained at $U_o/C_o=-0.20$ by S3D model is 86.86% smaller load than 3D model. Again for minimum load, S3D model yields 82.0% smaller load than 3D model. These results are summarized in Table 6. For the 3D oblique case we have not proceeded after $U_o/C_o=1.359$ since wave height at this current becomes negligible.

5. Implementation of the 2D and 3D model for layered surface current

In this study it is assumed that current is uniform and acting over a layer of fluid that extends from the free surface to a specified finite depth (Zaman and Baddour, 2005). The definition sketch of the domain is shown in Fig. 8. In this computation, we calculate the loads imparted by the fluid on a bottom mounted slender vertical cylinder representing a typical element of an offshore structure. The load computation uses Morison's equation with appropriate drag and mass coefficients. See for example Chakrabarti (1987, 2005) and Sarpkaya and Isaacson (1981).

5.1. Moment due to combined wave–current field on the slender cylinder about the bottom

Moment is computed for the interaction of waves with uniform currents of different layers acting down from the free surface, see Fig. 8.

The following equation is utilized in this case to compute the moment on the cylinder:

$$M_t = \int_{-d}^{\eta} \Delta\vec{F}_t \times (d+z)dz \tag{64}$$

Table 6
Loads for 3D case: wave with opposing current.

	U_o/C_o	F_t/F_w[a]	%
3D model	−0.20	6.219	
S3D model	−0.20	0.816	86.86 (−)
	U_o/C_o	F_t/F_w[b]	%
3D model	−0.20	−6.575	
S3D model	−0.20	−1.183	82.00 (−)

[a] Normalized maximum load.
[b] Normalized minimum load.

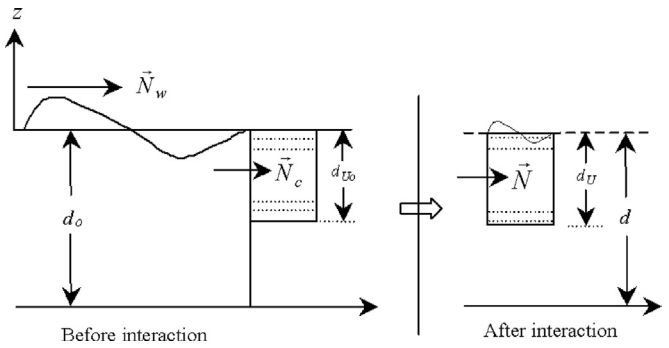

Fig. 8. Schematic view of 2D wave-free current and current-free wave field before and after interaction.

where $\Delta\vec{F}_t$ is the load/unit length of the cylinder and M_t is the total moment due to the load about the bottom of the cylinder, positive in the clockwise direction.

5.2. Computational procedure

In the present computations, the total loads are calculated from the effects of the combined wave–current field. The first step is to use Eqs. (6)–(23), (43), (47), (52) and (57) to predict the wave–current parameters that define the wave–current field. The second step in the computation is then to use Eq. (61) to produce the total load exerted on the cylinder by the combined wave–current field obtained in the first step. The third and the final step is to use Eq. (64) (see also Table 10) to compute the moment about the bottom of the cylinder.

5.3. Case study: Computations of loads and moments by 2D and 3D models

5.3.1. Load and moment computation by the 2D model for layered surface currents

As an example, the established model has been applied for the computation of loads for a collinear or 2D case and for an oblique or 3D case. For both examples, it is assumed that a monochromatic current-free surface wave interacts with a normalized wave-free uniform current U_o/C_o varying over the range of an opposite current to a range of following currents. It is also assumed that the layered current is uniform and acting over a layer of fluid that extends from the free surface to a specified finite depth. The extent of this layered-current is defined by the ratio of the layered-current depth, d_U to the mean water depth, d and may be described by the ratio d_U/d, see Fig. 8. The wave and current parameters used in this study are shown in Table 7. The diameter of the cylinder is 35 cm in all computations. Here the total loads and moments are calculated from the effects of the combined wave–current field as proposed above.

Descriptions of maximum and minimum loads are obtained by the above model for 2D collinear, non-oblique case are given in

Table 7
Computational parameters.

Parameters	2D model	3D model
U_o/C_o (*Maximum opposing*)	−0.20	−0.20
U_o/C_o (*Maximum following*)	0.572	1.359
H_o/L_o	0.01	0.01
d_o/L_o	2.0	2.0
d_U/d (*Maximum*)	1.0	1.0
d_U/d (*Minimum*)	0.25	0.25
Wave incident direction	0°	10°
Current incident direction	0°	15°

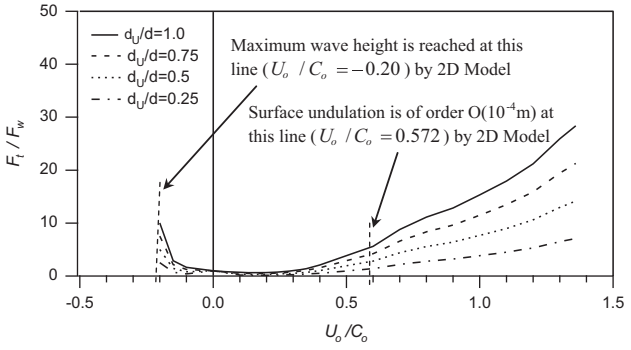

Fig. 9. Normalized maximum exerted loads computed by the 2D Model for different layered currents.

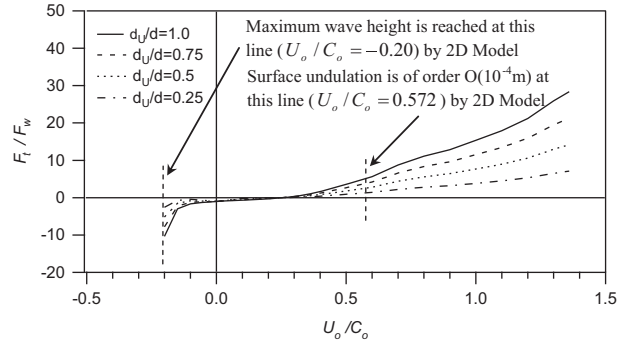

Fig. 10. Normalized minimum exerted loads computed by the 2D Model for different layered currents.

Figs. 9 and 10, respectively. In the 2D case we have found that the monochromatic wave that we have used in our computation, becomes $O(10^{-4}$ m) (with respect to incident wave) when normalized current parameter reaches the value $U_o/C_o=0.572$ for the case of a wave with a following current.

For the case when wave and current are in opposite directions the maximum wave height is reached at $U_o/C_o=-0.2$. Maximum wave height is reached due to wave blocking. At this point wave steepness exceeds the allowable breaking value ($\sim$0.14) and the numerical model is stopped. These limits are shown in Figs. 9 and 10 by a vertical dotted line. The analyses and comparisons of loads for 2D non-oblique case are again made at these two points, that is, when $U_o/C_o=0.572$ and $U_o/C_o=-0.20$.

On the other hand when wave and current are in opposite directions the maximum and minimum loads obtained at $U_o/C_o=-0.20$. The differences among the maximum and minimum moments computed by the 2D model for different layered currents are shown in Figs. 13 and 14, respectively. Tables 8a and 8b show the results of the loads and moments when the layered current is extended from the free surface to the bottom of the

Table 8a
Loads for 2D case: waves with following currents.

Load	U_o/C_o	F_t/F_w	M_t/M_w
Maximum	0.572	5.614	−5.621
Minimum	0.572	5.614	−5.621

Table 8b
Loads for 2D case: waves with opposite currents.

Load	U_o/C_o	F_t/F_w	M_t/M_w
Maximum	−0.20	10.029	−10.012
Minimum	−0.20	−10.389	10.407

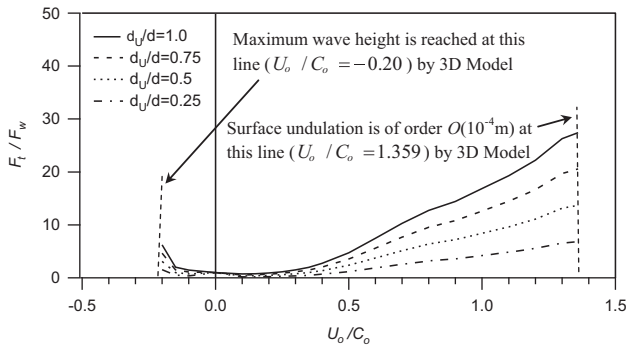

Fig. 11. Normalized maximum exerted loads computed by the 3D Model for different layered currents.

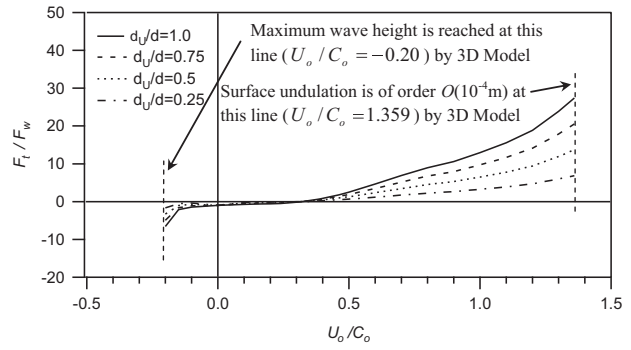

Fig. 12. Normalized minimum exerted loads computed by the 3D Model for different layered currents.

domain. Table 8a shows the results of the waves with the following currents while Table 8b represents the results of the waves with the opposing currents.

In the figures M_t stands for the total moment due to combined wave–current field or due to wave-free current field. M_w describe the absolute moment due to the current-free wave field.

5.3.2. Load and moment computation by the 3D model for layered surface currents

For the oblique interaction cases the above mentioned wave and current conditions are used (as shown in Table 1) and in addition, it is assumed that the wave enters the computational domain at an oblique angle of 10°, while the current is at an angle of 15° with the positive direction of the *x*-axis. Figs. 11 and 12 demonstrate the comparison between the maximum and minimum loads obtained by the above 3D model for different layered

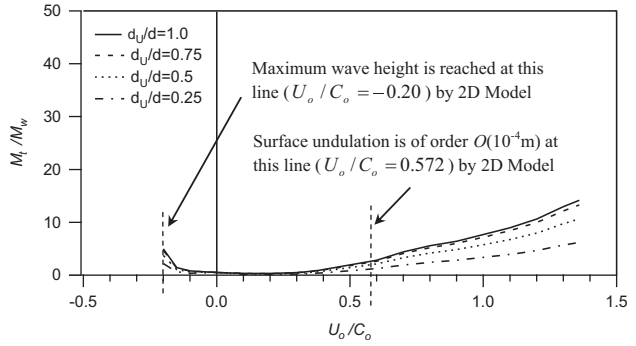

Fig. 13. Normalized maximum moments computed by the 2D model for different layered currents.

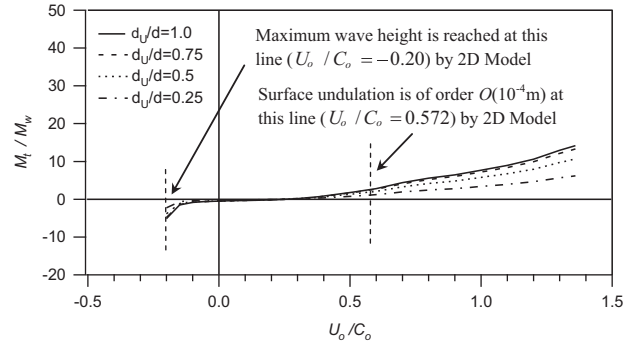

Fig. 14. Normalized minimum moments computed by the 2D model for different layered currents.

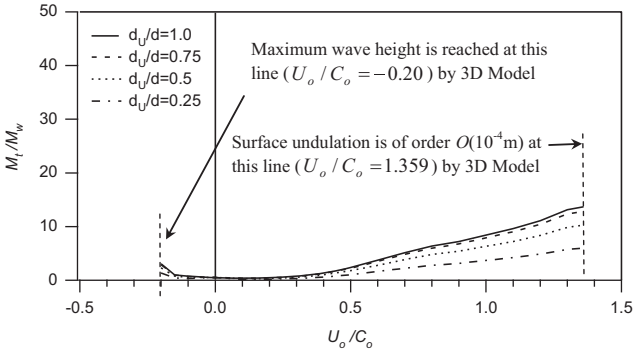

Fig. 15. Normalized maximum moments computed by the 3D model for different layered currents.

current depth. The comparisons among maximum and minimum moments computed by the 3D model for different layered currents are shown in Fig. 15 and in Fig. 16, respectively. In the 3D oblique case, the analyses of loads and moments are also made at two points, at $U_o/C_o=1.359$ when surface elevation is of $O(10^{-4}$ m) due to a wave with a following current and at $U_o/C_o=-0.20$ when the wave is in opposite direction of the current shown by vertical dotted line in Figs. 11 and 12.

In the absence of wave(s) the model still compute the loading imparted by the wave-free current field shown in the figures after the vertical dotted line.

On the other hand, when wave and current are in opposite directions the maximum and minimum loads and moments are obtained at $U_o/C_o=-0.20$. For the 3D oblique case we have not proceeded after $U_o/C_o=1.359$ since the wave height at this current becomes $O(10^{-4}$ m). Tables 9a,b represent the maximum and minimum loads and moments for $U_o/C_o=1.359$ and $U_o/C_o=-0.20$. In this case also, Tables 9a and 9b show the results of the loads and

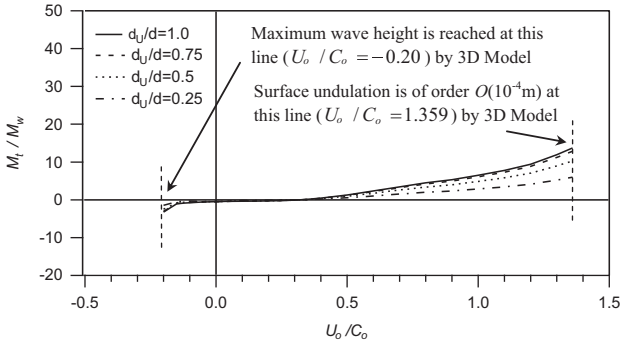

Fig. 16. Normalized minimum moments computed by the 3D model for different layered currents.

Table 9a
Loads for 3D case: waves with following currents.

Load	U_o/C_o	F_t/F_w	M_t/M_w
Maximum	1.359	26.280	−27.458
Minimum	1.359	23.856	−27.458

Table 9b
Loads for 3D case: waves with opposite currents.

Load	U_o/C_o	F_t/F_w	M_t/M_w
Maximum	−0.20	6.219	−6.295
Minimum	−0.20	−6.575	6.654

moments when the layered current is extended from the free surface to the bottom of the domain. Table 9a describes the results of the waves with the following currents and Table 9b represents the results of the waves with the opposing currents.

5.3.3. Moment computation by 2D model for layered surface currents

Figs. 13 and 14, respectively, show the maximum and minimum moment for 2D flow fields computed by Eq. (64) for the cases when waves coexist with a surface current that is uniform and acting over a layer of fluid that extends from the free surface to a specified finite depth. The total moment due to combined wave and layered current field M_t is normalized by the moment due to wave only M_w. The moment arms (M_a) for various wave and layered currents are computed by Eq. (64) shown in Table 10.

5.3.4. Moment computation by 3D model for layered surface currents

Figs. 15 and 16 respectively show the maximum and minimum moment for 3D flow fields computed by Eq. (64) for the cases when waves coexist with a surface current that is uniform and acting over a layer of fluid that extends from the free surface to a specified finite depth. In the figures total moment due to combined wave–current field M_t is normalized by the moment due to wave M_w.

6. Conclusion

A 3D numerical model has been developed using three-dimensional expressions describing the characteristics of the combined wave–current field in terms of mass, momentum and energy flux conservation equations. The obtained model is then employed for the computation of the resulting combined

Table 10
Moment arms (M_a) to depth (d) to compute moment.

U_o/C_o	M_a/d ($d_U/d=1.0$)	M_a/d ($d_U/d=0.75$)	M_a/d ($d_U/d=0.50$)	M_a/d ($d_U/d=0.25$)
−0.2	0.496772	0.621	0.745158	0.869352
−0.15	0.498201	0.622	0.747301	0.871852
−0.1	0.499203	0.624	0.748804	0.873605
0	0.5	0.5	0.5	0.5
0.1	0.5	0.624	0.75	0.875
0.15	0.5	0.625	0.75	0.875
0.2	0.5	0.625	0.75	0.875
0.25	0.5	0.625	0.75	0.875
0.3	0.5	0.625	0.75	0.875
0.35	0.5	0.625	0.75	0.875
0.4	0.5	0.625	0.75	0.875
0.5	0.5	0.625	0.75	0.875
0.6	0.5	0.625	0.75	0.875
0.7	0.5	0.625	0.75	0.875
0.8	0.5	0.625	0.75	0.875
0.9	0.5	0.625	0.75	0.875
1	0.5	0.625	0.75	0.875
1.1	0.5	0.625	0.75	0.875
1.2	0.5	0.625	0.75	0.875
1.3	0.5	0.625	0.75	0.875
1.359	0.5	0.625	0.75	0.875

wave–current field direction and kinematics and total loading on a slender vertical cylinder in 2D and in 3D flow field. Eqs. (31)–(36) produce the governing conservation equations when Eqs. (26), (28) and (30) are used to formulate the unknown quantities for the cases of wave, current and wave–current conditions. The obtained equations are used for the numerical computation of the combined field parameters. Maple-12 (2008) software environment is used for the iterative solution of the nonlinear system of conservation equations and free-surface dispersion relation. In the computations the direction of the combined wave–current field and, after-interaction surface disturbance height H, its length L, mean water depth d and current like parameter U are computed. Examples for collinear 2D non-oblique waves and currents and an oblique 3D case are shown. The present 2D and 3D combined wave–current models are compared with S2D and S3D superposition models. The comparisons show that superposition models are less effective for the computations of loads especially when waves and currents have opposite directions. Four different categories of current field considering its extent from the free surface to a certain water depth are also considered for load and moment computation by the numerical 2D and 3D numerical models. It is observed as expected that total load on the vertical cylinder is directly proportional to d_U/d ratios, *i.e.* when d_U/d is greater the loading on the cylinder is also larger. Similar phenomenon is observed for moments of different current depths from the free surface. It is necessary to mention here that for the case of wave with following current, even when waves disappear due to strong current, the present model is still applicable for the computation of loading due to current only. In another words this 3D (also 2D) model is capable to compute loads in the presence of current only cases.

References

Baddour, R.E., Song, S.W., 1990a. On the interaction between waves and currents. Ocean Eng. 17 (1/2), 1–21.

Baddour, R.E., Song, S.W., 1990b. Interaction of higher-order water waves with uniform currents. Ocean Eng. 17 (6), 551–568.

Chakrabarti, S., 2005. Handbook of Offshore Engineering. 1. Elsevier p. 661

Chakrabarti, S.K., 1987. Hydrodynamics of Offshore Structures. Computational Mechanics Publication, Springer-Verlag, pp. 1–440.

Dean, R.G., Dalrymple, R.A., 1992. Water Wave Mechanics for Engineers and Scientists. Prentice-Hall Inc, Englewood Cliffs, NJ, pp. 66–69.

Hedges, T.S., Lee, B.W., 1991. The equivalent uniform in wave–current computations. Coastal Eng. 16, 301–311.

Iwagaki, Y., Asano, T., Nagai, F., 1983. Hydrodynamic forces on a circular cylinder placed in the wave–current co-existing fields, Memoirs of the Faculty of Engineering. Kyoto University, Japan, XLV, pp. 11–23.

Kemp, P.H., Simons, R.R., 1982. The interaction between waves and a turbulent current: waves propagating with the current. J. Fluid Mech. 116, 227–250.

Kemp, P.H., Simons, R.R., 1983. The interaction of waves and a turbulent current: waves propagating against the current. J. Fluid Mech. 130, 73–89.

Longuet-Higgins, M.S., Stewart, R.W., 1960. Changes in the form of short gravity waves on long waves and tidal currents. J. Fluid Mech. 8, 565–583.

Longuet-Higgins, M.S., Stewart, R.W., 1961. The changes in amplitude of short gravity waves on steady non-uniform currents. J. Fluid Mech. 10, 529–549.

Maple-12, 2008. Language Reference Manual. Waterloo Maple Publishing, Springer-Verlag, Heidelberg, NY p. 2008.

Morison, J.R., O'Brien, M.P., Johnson, J.W., Schaaf, S.A., 1950. The forces exerted by surface waves on piles. Pet. Trans., AIME 189, 149–157.

Sarpkaya, T., Isaacson, M., 1981. Mechanics of Wave Forces on Offshore Structure-sVan Nostrand Reinhold Company Inc1–651.

Thomas, G.P., 1981. Wave–current interactions: an experimental and numerical study. Part 1. Linear waves. J. Fluid Mech. 110, 457–474.

Whitham, G.B., 1962. Mass, momentum and energy flux in water waves. J. Fluid Mech. 12, 135–147.

Zaman, M.H., Togashi, H., Baddour, E., 2010. Interaction of waves with non-colinear currents. Ocean Eng. 38 (4), 541–549.

Zaman, M.H., Togashi, H., Baddour, E., 2008. Deformation of monochromatic water waves propagating over a submerged obstacle in the presence of uniform current. Ocean Eng. 35 (8–9), 823–833.

Zaman, M.H., Baddour, R.E., 2006. Wave–current loading on a vertical slender cylinder by two different numerical models. In: Twenty-fifth International Conference on Offshore Mechanics and Arctic Engineering (OMAE-2006), ASME, Hamburg, Germany, pp. 8, on CD-ROM.

Zaman, M.H., Baddour, R.E., 2005. Combined loading of a wave and surface current on a fixed vertical slender cylinder. In: Twenty-fourth International Conference on Offshore Mechanics and Arctic Engneering, OMAE-2005, ASME, Halkidiki, Greece, pp. 8, on CD-ROM.

Zaman, M.H., Baddour, R.E., 2004. Loading on a fixed vertical slender cylinder in an oblique wave–current field. In: Twenty-third International Conference on Offshore Mechanics and Arctic Engneering (OMAE-2004), ASME, Vancouver, pp. 9, on CD-ROM.

Zaman, M.H., Baddour, R.E., 2003. Wave–current loading on a vertical cylinder. Fluid Struct. Interact. II, J. Adv. Fluid Mech., 43–52.

Zaman, M.H., Baddour, R.E., 2002. Waves and currents interacting in a 3D field. In: International Conference on Ship and Ocean Technology (SHOT-2002), IIT-Kharagpur, India, (on CD-ROM).

Zaman, M.H., Togashi, H., 1996. Experimental study on interaction among waves, currents and bottom topography. Proc. Civ. Eng. Ocean, JSCE 12, 49–54.